3D porous hybrids of defect-rich MoS_2/graphene nanosheets with excellent electrochemical performance as anode materials for lithium ion batteries

Longsheng Zhang,[a] Wei Fan,[a] Weng Weei Tjiu,[b] and Tianxi Liu*[a]

Electronic Supplementary Information

Fig. S1 FESEM image of bulk MoS_2. The digital image (inset) shows the poor dispersibility of bulk MoS_2 in aqueous solution (3 mg mL^{-1}).

Fig. S2 FESEM images of dr-MoS_2 NSs (a) before and (b) after the thermal reduction process.

Fig. S3 TEM images of dr-MoS_2 NSs (a) before and (b) after the thermal reduction process.

Fig. S4 (a) TEM and (b) HRTEM images of df-MoS_2 NSs.

Fig. S5 FESEM images, corresponding EDX spectra and EDX mapping images of (a) dr-MoS_2/GNS (2:1), (b) dr-MoS_2/GNS (6:1) and (c) dr-MoS_2/GNS (10:1) hybrids.

Fig. S6 XRD patterns of dr-MoS_2 NSs before and after the thermal reduction process.

Fig. S7 (a) XPS survey spectrum and (b) high resolution C 1s spectrum of GO sheets.

Fig. S8 First three discharge and charge curves of GNS in the voltage range from 0.01 to 3.0 V at a current density of 0.1 A g^{-1}.

Fig. S9 Comparison of the cycling performance of dr-MoS_2 NSs, df-MoS_2 NSs and bulk MoS_2 at a current density of 0.1 A g^{-1}.

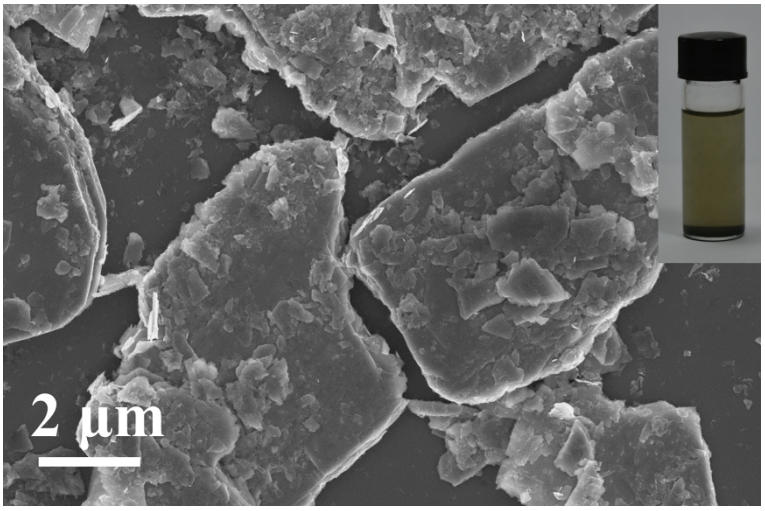

Fig. S1

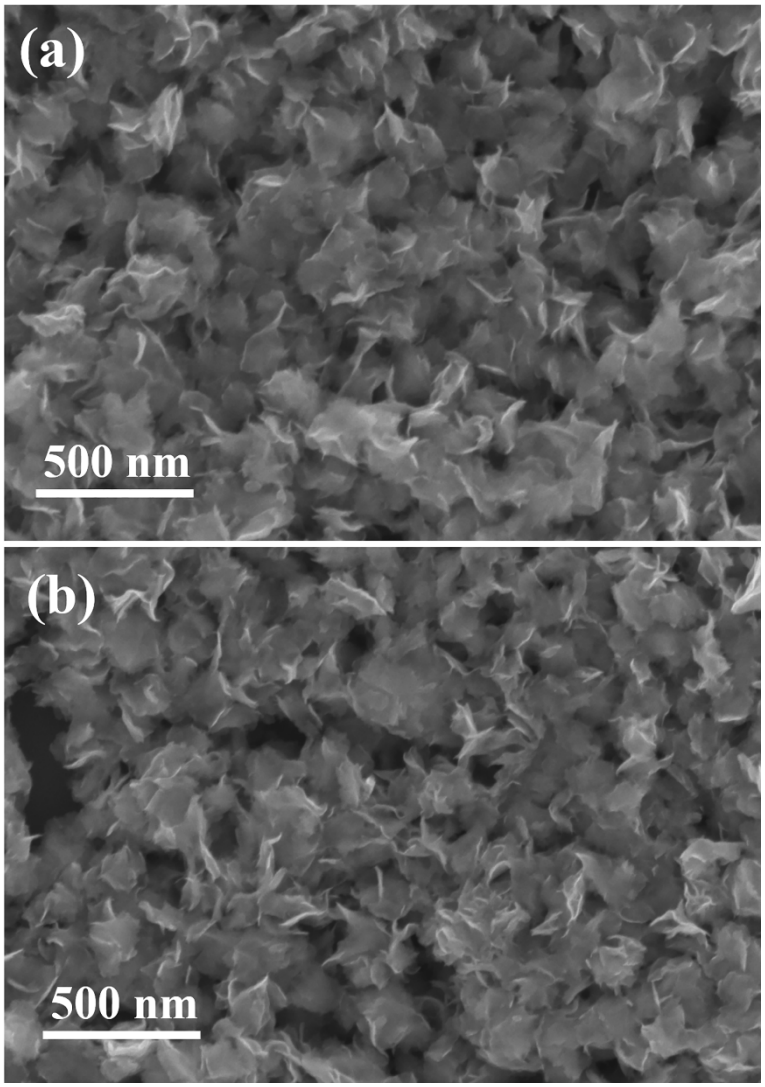

Fig. S2

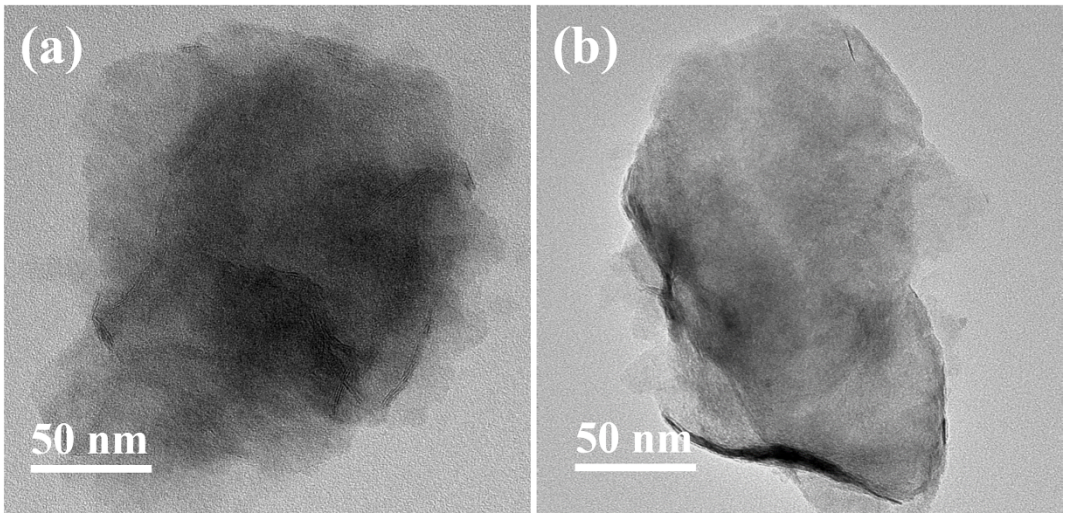

Fig. S3

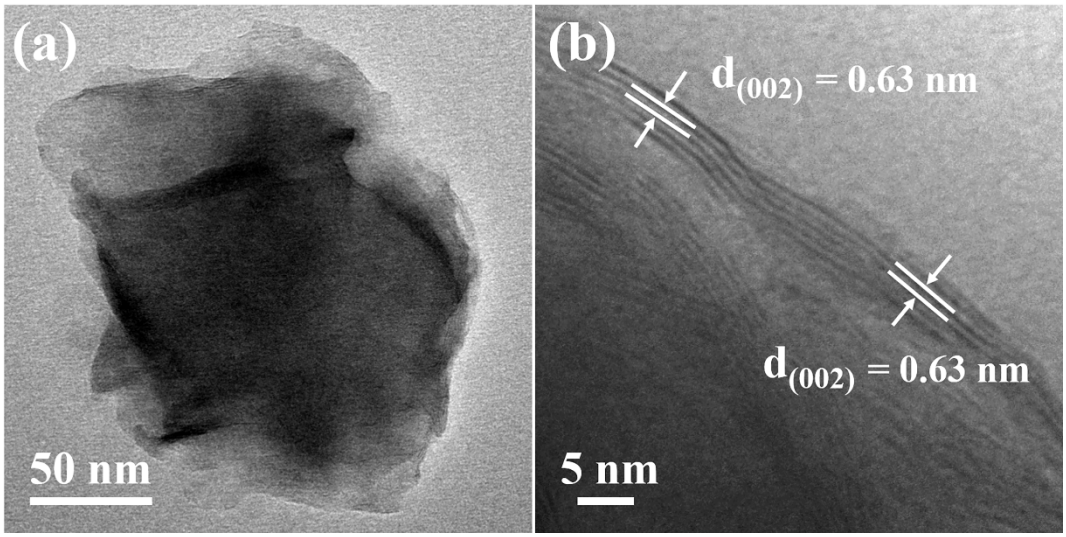

Fig. S4

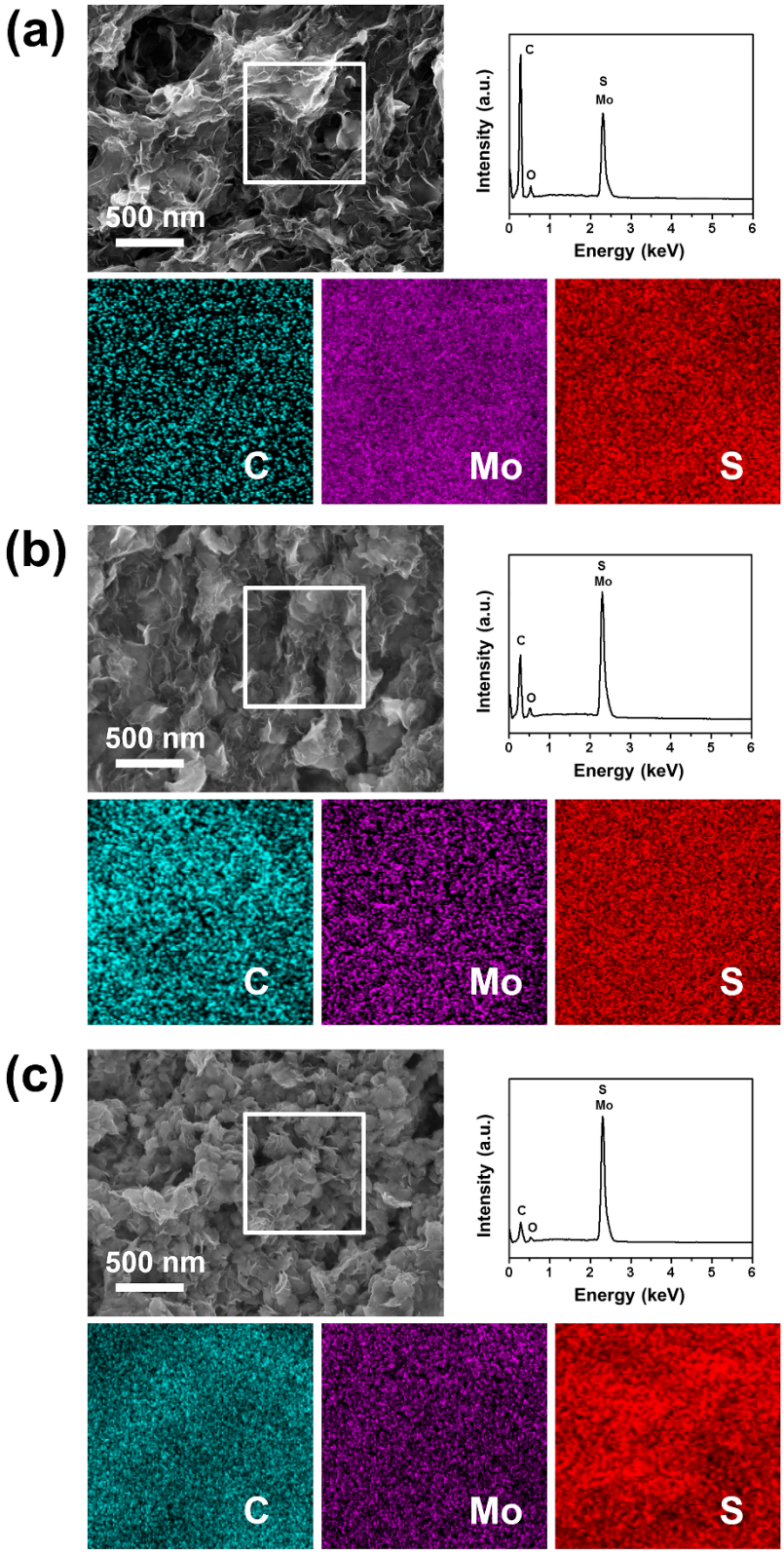
(a)
500 nm
C
S
Mo
O
Intensity (a.u.)
Energy (keV)
C
Mo
S
(b)
500 nm
C
S
Mo
O
Intensity (a.u.)
Energy (keV)
C
Mo
S
(c)
500 nm
C
S
Mo
O
Intensity (a.u.)
Energy (keV)
C
Mo
S

Fig. S5

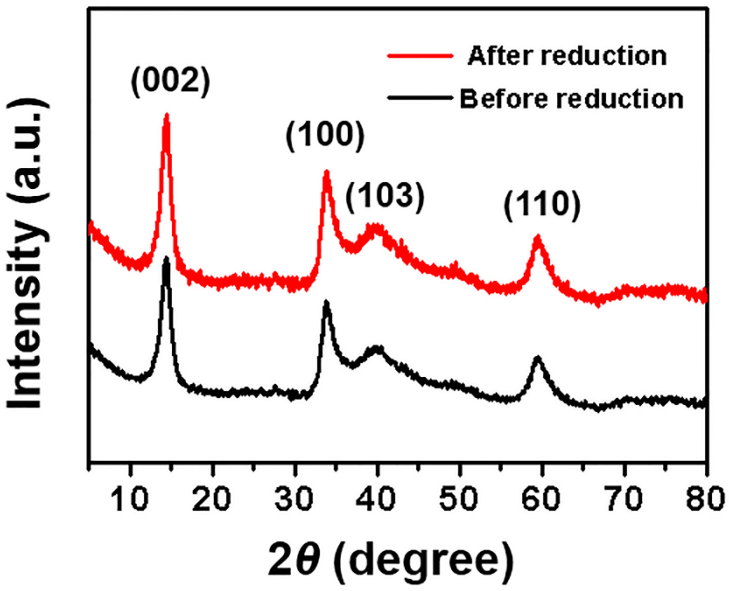
After reduction
Before reduction
(002)
(100)
(103)
(110)
Intensity (a.u.)
10
20
30
40
50
60
70
80
2θ (degree)

Fig. S6

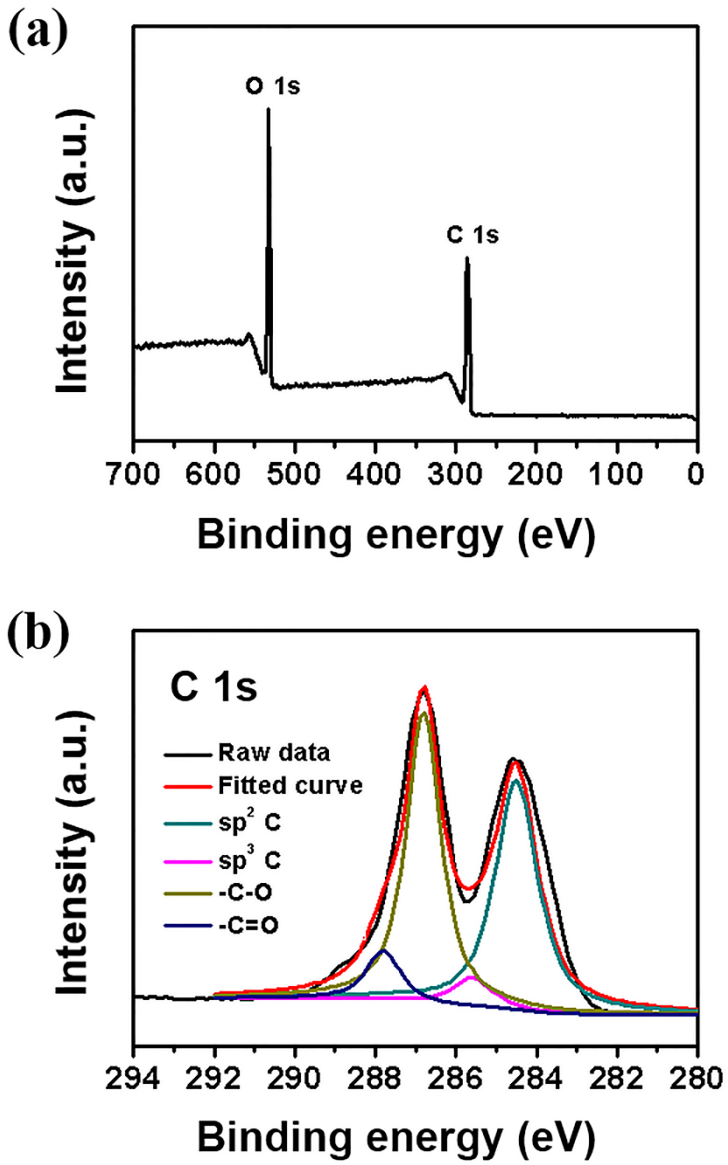
(a)
O 1s
C 1s
Intensity (a.u.)
700 600 500 400 300 200 100 0
Binding energy (eV)
(b)
C 1s
Raw data
Fitted curve
sp2 C
sp3 C
-C-O
-C=O
Intensity (a.u.)
294 292 290 288 286 284 282 280
Binding energy (eV)

Fig. S7

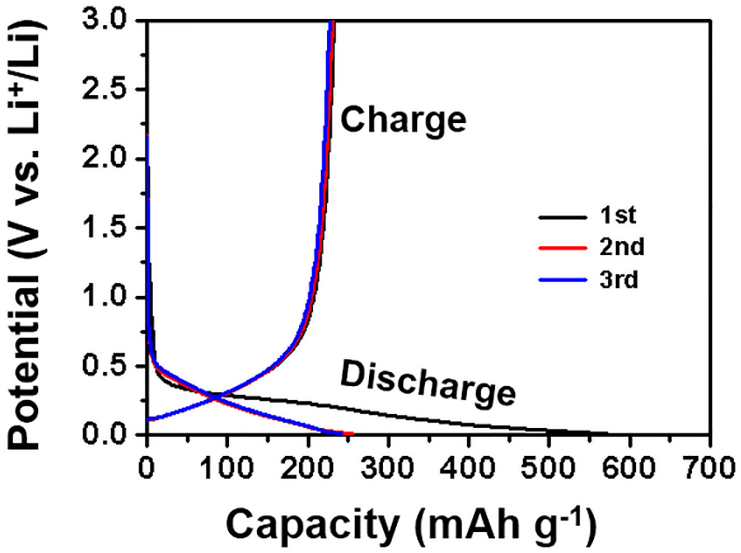
Potential (V vs. Li+/Li)
3.0
2.5
2.0
1.5
1.0
0.5
0.0
0
100
200
300
400
500
600
700
Capacity (mAh g-1)
Charge
Discharge
1st
2nd
3rd

Fig. S8

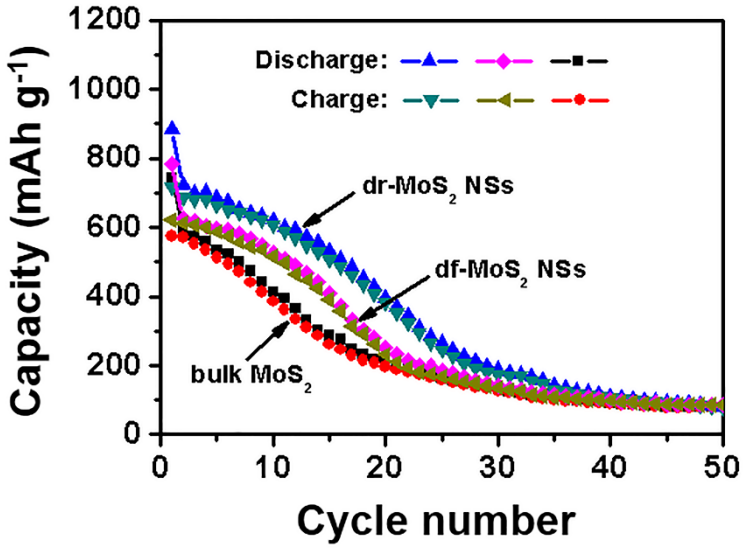
Discharge:
Charge:
dr-MoS2 NSs
df-MoS2 NSs
bulk MoS2
Capacity (mAh g-1)
Cycle number
0
200
400
600
800
1000
1200
0
10
20
30
40
50

Fig. S9